THE ASTROPHYSICAL JOURNAL, 298:651–659, 1985 November 15

PREIONIZATION-DEPENDENT FAMILIES OF RADIATIVE SHOCK WAVES

DONALD P. COX[1]
Department of Space Physics and Astronomy, Rice University
AND
JOHN C. RAYMOND[2]
Harvard-Smithsonian Center for Astrophysics
Received 1985 January 14; accepted 1985 May 17

ABSTRACT

Radiative shock waves are shown to be organizable into families within which the spectra are very similar. Each family contains a range of shock velocities, each member corresponding to a different degree of preionization in gas entering the shock. The covariation between shock velocity and preionization is such that the constant among a family's members is the enthalpy per atom at the epoch at which the very rapid collisional ionization of hydrogen and neutral helium is complete in the postshock flow. The spectral differences among members of one family derive from collisional excitation of neutral hydrogen and helium in the "hydrogen ionization zone" just inside the shock front. Signatures of preshock neutrals are thus found in the brightness (and perhaps the decrement) of the Balmer lines, in the intensity of the two-photon continuum, and in the ratio of He I singlet to triplet lines.

Representative spectra of four families are calculated using a newly revised spectral code. The differences between families are marked; with a finer grid of calculations there should be no difficulty identifying the family membership of an observed spectrum, although UV observations are required at high shock velocities. All family spectra were calculated at the same ram pressure, minimizing differences in the optical spectra due to varying degrees of collisional de-excitation. Future use of this technique will distinguish spectral differences due to "shock velocity" from those due to recombination zone density.

Subject heading: shock waves

I. INTRODUCTION

The spectra of fully developed radiative shock waves depend on a number of parameters, particularly the shock velocity and preshock values of the density, ionization level, magnetic field, grain constituency, and elemental abundances. One of the more problematic of these parameters, the preshock ionization level, was studied by Shull and McKee (1979) with the intent of eliminating it as an unknown. In particular, they assumed that the preshock ionization should be in equilibrium with the radiation field of the shock itself, and calculated the corresponding level. Unfortunately, the recombination time scale ($\sim 10^5$ yr/density [in cm^{-3}]) is very often much larger than the dynamical evolution time scale in systems of interest, and the equilibrium ionization level is then inappropriate. A case in point is the recent simple model by Blair and Raymond (1984) of a shock wave slowing as it enters an interstellar cloud (density increasing from 2 to 10 cm^{-3} over a distance of 1 pc). Their result is that preshock gas is at first ($v_s > 150$ km s^{-1}) severely underionized compared with equilibrium and later ($v_s < 110$ km s^{-1}) severely overionized. A supernova remnant evolving in a homogeneous medium behaves in the same manner (Cox 1972). Whenever shock velocities are changing rapidly, such hysteresis in ionization will be marked.

Rather than eliminating the preionization as a parameter, we show below that shocks with different preionization levels and shock velocities can be organized into spectrally similar families. We will show that a high-velocity shock into neutral material is spectrally similar to a somewhat slower shock in fully ionized material. These similarities should allow the identification of the family to which an observed spectrum belongs, while spectral details permit subsequent identification of the separate values of shock velocity and preionization.

Because forbidden line cooling rates are density sensitive, the density in the recombination zone affects optical spectra. By calculating shock spectra for the various families at constant recombination zone density, rather than constant preshock density, we are able to separate the effects of "velocity" (by which we mean postionization enthalpy per atom) from those of "density" (by which we mean the degree of collisional de-excitation in the optical lines).

II. THE FAMILY CONCEPT AND COMPOSITE SPECTRA

The physical structure of a radiative shock consists of several distinct regions. The ambient gas, already perturbed somewhat by the precursive radiation field, meets first an adiabatic shock transition to a high-temperature state. If neutrals are present in the immediate postshock environment, then for shock velocities $v_s > 100$ km s^{-1}, the collisional excitation and ionization of those neutrals take place at far and away the dominant rates. Just inside the shock there is thus a very thin zone containing neutrals in the process of being ionized. Slightly downstream of this "hydrogen ionization zone," hydrogen is fully ionized, helium is at least singly ionized, and all other elements are scrambling toward multiple ionization. (Owing to their low abundances, the preionization of heavier elements is unimportant, unless it is so severe that it approaches the ioniz-

[1] On leave from the Department of Physics, University of Wisconsin at Madison.

[2] Guest observer with the *International Ultraviolet Explorer* satellite, which is jointly operated by the US National Aeronautics and Space Administration, the Science Research Council of the UK, and the European Space Agency.

ation level achieved in the cooling zone.) This begins the far more extended but optically thin "cooling region" within which the overall ionization level rises and then falls as the gas radiatively cools to $\sim 10^4$ K. The radiated enthalpy is converted primarily to UV photons, many beyond the Lyman limit. That region is then followed by a "photoionized (or recombination) zone" with a temperature of several thousand kelvins and a comparatively high density (the pressure being slightly higher than the postshock value while the temperature is very much lower). In this zone, roughly half of the ionizing continuum generated by the cooling region is fluoresced to produce the low-excitation portion of the optical spectrum. (Radiation from O^{++} is produced primarily in the cooling zone, from O^+ in the transition between the cooling and photoionized zones, while the Balmer, low-excitation ion, and neutral spectra derive from the photoionized zone.)

It is clear that to the extent that the hydrogen ionization and cooling zones are segregated, their spectra can be segregated as well. Consider first the ionization zone spectrum which we denote S_1. Owing to their dominant abundances, hydrogen and helium excitation dominate the production of S_1 during their brief ionization episode. Furthermore, the relative constancy of the ratio of collisional excitation to ionization cross sections at high temperature makes the S_1 spectrum linear in the number of neutrals present, and insensitive to the temperature. To a first approximation, there is only one S_1 spectrum, present in an amount proportional to the preshock neutral content.

The collisional excitation of singly ionized helium is extremely important to the overall cooling, but being slower than the collisional excitation of neutral hydrogen and helium, lumping the associated processes into the cooling zone gives a reasonable approximation.

The net effects of the hydrogen ionization zone are to complete the ionization of hydrogen and neutral helium, produce the S_1 spectrum, and reduce the enthalpy per atom reaching the cooling region. Thus, just subsequent to this zone the flow is fully ionized with a temperature which is lower (considerably lower if the preshock neutral content was high) than the postshock value.

The gas does not know or care how it reached that state. An entirely different shock, proceeding into completely preionized material, would produce, for suitably chosen shock velocity and preshock density, a postshock flow with exactly the same enthalpy per particle and stagnation pressure. The subsequent evolution of both flows is essentially identical, as is the subsequent spectrum. Subdividing this spectrum into that due to the cooling region, S_2, and that due to the photoionized zone, S_3, the S_2 spectrum is even independent of the chosen density. There is thus a one-dimensional family of S_2 spectra (depending on postionization enthalpy) and a two-dimensional family of S_3 spectra (depending also on recombination zone density).

The above discussion has been idealized for clarity. There is no clear boundary between the hydrogen ionization zone and the cooling region; some of the S_1 spectrum consists of photons energetic enough to contribute to the ionization fluorescence of S_3, and the flow conditions emerging from the hydrogen ionization zone are not identical to any reached by a strong shock even at the same enthalpy and pressure. A further idealization, the assumption of equal electron and ion temperatures, is discussed in § V. The subsequent thrust of this paper is to find the idealized family relationship between shocks of different v_s and preionization but the same S_2 spectra, and then using a full radiative shock wave code, to demonstrate the usefulness of the idealization.

III. ENTHALPY EVOLUTION AND SPECTRUM OF THE HYDROGEN IONIZATION ZONE

The calculation of the enthalpy loss and the S_1 spectrum from the ionization zone is very straightforward. One basically simplifies a standard shock cooling program to include only processes involving neutral helium and hydrogen. The evolutions from given initial neutral fractions then terminate at that value of enthalpy consistent with full single ionization (given that the shock velocity is high enough to achieve it—see below). Such calculations in fact evolve through a continuous family of enthalpies and ionizations, all of which as initial conditions would produce the same fully ionized state.

In the equations to follow, the hydrogen and helium number densities are $n_{\rm H}$ and $n_{\rm He} = An_{\rm H}$, where A is the relative abundance. The ion density is then $n = (1 + A)n_{\rm H}$. The corresponding neutral fractions are defined as, $g_{\rm H}$ and $g_{\rm He}$, making the electron density

$$\begin{aligned} n_e &= (1 - g_{\rm H})n_{\rm H} + (1 - g_{\rm He})n_{\rm He} \\ &= [(1 - g_{\rm H}) + A(1 - g_{\rm He})]n/(1 + A) . \end{aligned}$$

The mass per ion is $m = (1 + 4A)m_{\rm H}/(1 + A)$, and the ionization energy density is

$$U_{\rm I} = [(13.6\ {\rm eV})(1 - g_{\rm H}) + (24.6\ {\rm eV})(1 - g_{\rm He})A]n/(1 + A) .$$

For the moment neglecting the magnetic field and preshock temperature, the initial enthalpy per nucleus is (with $I_{\rm H} = 13.6$ eV and $I_{\rm He} = 24.6$ eV)

$$h_0 = \frac{mv_s^2}{2} + \frac{I_{\rm H}[1 - g_{\rm H}(0)] + AI_{\rm He}[1 - g_{\rm He}(0)]}{1 + A} .$$

In the ionization zone, $g_{\rm H}/(1 + A)$ ionizations of hydrogen and $g_{\rm He}A/(1 + A)$ of helium take place per average nucleus. To the extent that the excitation and ionization cross sections maintain the same proportion, the excitation energy lost per net ionization is constant, $R_{\rm H}$ for hydrogen and $R_{\rm He}$ for helium. The postionization enthalpy is thus

$$\begin{aligned} h_i = &\frac{mv_s^2}{2} + \frac{I_{\rm H} + AI_{\rm He}}{1 + A} \\ &- \frac{g_{\rm H}(0)(R_{\rm H} + I_{\rm H}) + Ag_{\rm He}(0)(R_{\rm He} + I_{\rm He})}{1 + A} , \end{aligned}$$

where the terms depending on $g_{\rm H}(0)$ and $g_{\rm He}(0)$ have been combined. Thus the shock velocity v_i that would produce the same final enthalpy in gas with full preionization is given by

$$v_i^2 = v_s^2 - \frac{2}{m}\left[\frac{g_{\rm H}(0)(R_{\rm H} + I_{\rm H}) + Ag_{\rm He}(0)(R_{\rm He} + I_{\rm He})}{1 + A}\right] .$$

Finally, by defining

$$v_H^2 = \frac{2}{m}\frac{R_{\rm H} + I_{\rm H}}{1 + A} , \quad v_{\rm He}^2 = \frac{2}{m}\frac{A(R_{\rm He} + I_{\rm He})}{1 + A} ,$$

we have

$$v_i^2 = v_s^2 - g_{\rm H}(0)v_{\rm H}^2 - g_{\rm He}(0)v_{\rm He}^2 .$$

TABLE 1

OUTPUT IN eV PER AVERAGE ATOM

MODE	VELOCITY				
	120	140	160	180	200
H ionization	12.7	12.8	12.8	12.7	12.7
Lyα	10.6	10.1	9.46	8.59	7.60
H two-photon[a]	4.71	4.20	3.40	3.34	3.29
Hα—case A	0.19	0.16	0.14	0.12	0.11
Hα—case B	0.45	0.42	0.41	0.40	0.39
Total H radiation	19.0	18.1	17.7	17.5	17.4
He ionization	2.26	2.28	2.29	2.30	2.31
He $1s2p\ ^1P$	0.63	0.50	0.43	0.40	0.38
He two-photon[b]	0.33	0.19	0.13	0.10	0.08
He triplets	0.70	0.35	0.22	0.16	0.13
Total He radiation	2.35	1.55	1.23	1.07	0.97

[a] Assumes case B.

[b] Only direct excitation to $1s2s\ ^1S$; total He two-photon will be larger depending on optical depth in $1s^2$–$1s2p$ singlet lines.

This equation contains (for constant v_i) the first-order effects relating shock velocities among family members. Each family can be characterized by its value of v_i, the equivalent shock velocity into fully ionized material, or alternatively by v_n, the shock velocity into fully neutral material. (The former is easiest to use in the above presentation, the latter easiest in later calculations.)

For high shock velocities, the linearity of the above approximate result rather accurately follows the results of the detailed calculations presented below. At lower velocities, however, the ratio of excitation to ionization cross section is sensitive to temperature, altering the simple form.

A computer program to follow the detailed evolution of enthalpy and emission from the hydrogen ionization zone was constructed as described in Appendix A, and a representative set of calculations were made. All began with $T_0 = 10^4$ K, $n_0/B_0 = 100\ \mathrm{cm^{-3}}\ \mu\mathrm{G}^{-1}$, and had $g_{\mathrm{H}}(0)$ and $g_{\mathrm{He}}(0) = 1$. Shock velocities ($v_s = v_n$ in these cases) were chosen at 20 km s^{-1} intervals from 80–200 km s^{-1}. The helium abundance was taken as $A = 0.1$. The low magnetic field was chosen to keep its effects small in the current exploration.

The total calculated radiative outputs for the hydrogen ionization zone of the five faster shocks are shown in Table 1. In each case the ionization drains should be 13.6/1.1 = 12.4 eV for hydrogen, and 24.6/11 = 2.24 eV for helium. The step size was such that the integrated values shown are typically 2%–3% high. The predicted Hα emission is given for two extreme assumptions: that all of the higher Lyman line photons escape (case A), or that all are converted through scattering to Lyα plus Balmer, Pashen, etc., lines (case B). Radiative transfer calculations (Chevalier, Kirshner, and Raymond 1980) show that the Hα emission is roughly midway between these extremes for high shock velocities, but approaches case B for slower shocks. The full radiative shock code results presented in the next section all assume case B. Note that the hydrogen two-photon emission was computed for case B.

Roughly speaking, collisional excitation of hydrogen is half again more effective than ionization as an enthalpy sink, while for helium, excitation is somewhat less effective. The typical total drains per average atom are ~30.5 eV for hydrogen and 3.5 eV for helium (with $A = 0.1$). Multiplying these by $2/m$ to estimate v_{H}^2 and v_{He}^2, we find the approximate family relationship

$$v_i^2 \approx v_s^2 - g_{\mathrm{H}}(0)(67.8\ \mathrm{km\ s^{-1}})^2 - g_{\mathrm{He}}(0)(23.0\ \mathrm{km\ s^{-1}})^2 .$$

Thus for $g_{\mathrm{H}}(0) = g_{\mathrm{He}}(0) = 1$, $v_s = v_n$, $v_i^2 \approx v_n^2 - (71.6\ \mathrm{km\ s^{-1}})^2$. The difference between v_i and v_n is small at high velocities (e.g., 187 vs. 200 km s^{-1}), but much more significant at lower velocities (e.g., 70 km s^{-1} vs. 100 km s^{-1}). In fact, however, at low velocities the relative importance of collisional excitation is so great that full ionization is never achieved. For $v_n \leq 100$ km s^{-1}, family membership does not extend to fully ionized members.

The temperature evolutions of the hydrogen ionization zones are shown in Figure 1. Between the far right-hand side, where the thermal enthalpy per ion is $5kT(1)/2$, and the left side, three things happen. The total enthalpy is initially a factor of 16/15 higher than the thermal enthalpy, the residual being kinetic energy. From this total enthalpy, 34 eV is subtracted by excitation and ionization [equivalent to 0.4 (34 eV)/k = 158,000 K] and then the residual enthalpy shared among twice as many particles. Owing to the compression and slowing accompanying the enthalpy drop, the residual enthalpy is almost entirely thermal. Thus $T(\mathrm{ionized}) \approx (\frac{1}{2})[(16/15)T(1) - 158{,}000\ \mathrm{K}]$. This result represents the variations very accurately for all $v_n \geq 100$ km s^{-1}, except for the sharp downturn of the $v_n = 100$ km s^{-1} curve near $g_{\mathrm{H}} = 0$.

The ionization relationships between the family members are shown in Figure 2. At very high temperatures helium is ionized slightly more rapidly than hydrogen, while for slower shocks and their lower temperatures, helium ionization lags progressively behind that of hydrogen.

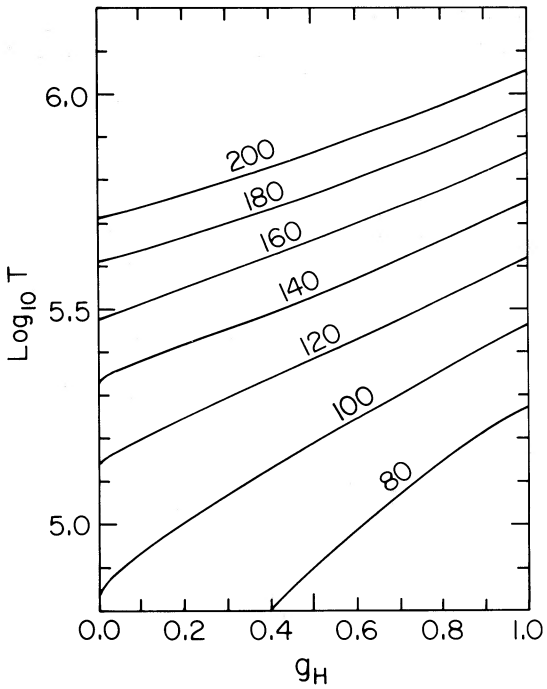

FIG. 1.—Evolution of temperature vs. hydrogen neutral fraction in the hydrogen ionization zone just inside the shock. Curves are labeled with v_n in units of km s^{-1}.

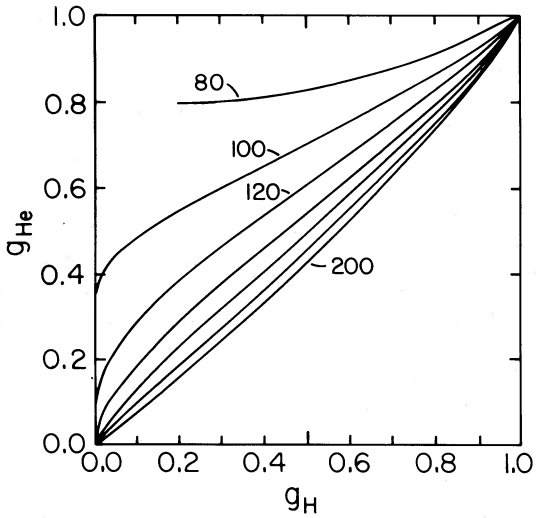

FIG. 2.—Evolution of helium vs. hydrogen neutral fraction in hydrogen ionization zone. Curves are spaced at 20 km s^{-1} intervals in v_n.

IV. FAMILY RELATIONSHIPS

The previous section provides the enthalpy, temperature, and ionization evolutions for the hydrogen ionization zone. It is still a matter of some taste to choose the best equivalent shock parameters. We have elected to match the postionization enthalpy, hydrogen and helium neutral fractions, the same ratio of magnetic field to density, the same stagnation pressure, and maintain the same preshock temperature. The equations for the inversion from the postionization conditions to the equivalent family member are straightforward and included in Appendix B.

The above inversion choice does not lead to exactly the same temperature, density, or flow velocity as in the postionization flow, essentially providing a somewhat higher proportion of kinetic energy and lower temperature. As a consequence, the spatial and temporal structures of the subsequent flows will differ, as will the ionization fractions of the very highest states achieved. What this choice does do is to preserve the total amount of energy per ion which is radiated in the S_2 spectrum. In addition, in the photoionization zone where kinetic energy is generally negligible, the equation of state at given temperature and ionization fraction is essentially identical, with thermal and magnetic pressures each equal among family members.

Specific family member preshock properties for several families are provided in Table 2, and the graph of equivalent shock velocity versus g_H for all families calculated is shown in Figure 3. (The corresponding values for g_{He} are those of Fig. 2.) In running the family code, $n_0 = 10$ cm^{-3} and $B_0 = 0.1$ μG were used in starting all calculations from neutral. The results shown in Table 2, however, have had their densities and magnetic fields scaled to provide a closer equivalence between ram pressures for the different v_n families. In the next section we present the calculated spectra for the conditions given in Table 2, all of which thus have closely similar densities in their photoionization zones.

The shock velocity trajectories in Figure 3 have a parabolic coordinate system—the vertical axis is linear in v_s^2 but calibrated in v_s, along the right-hand edge. The left-hand scale displays $v_7^2 \equiv (v_s/100 \text{ km s}^{-1})^2$. The approximate analysis (based on the typical loss of 34 eV per ionization) suggested that $v_7^2 \approx (v_n/100 \text{ km s}^{-1})^2 - 0.5(1 - g)$ would be found. The average slope of 0.5 is certainly evident in Figure 3, but it is also clear that at lower velocities the slope increases somewhat, showing the greater relative importance of collisional excitation at lower temperatures.

The family curves of Figure 3 are sufficiently well behaved and insensitive to modest variations in the helium ionization that they should prove almost universally valid, so long as the shocks are strong enough that T_0 and B_0 have little effect in the initial jump.

Cox (1972), Raymond (1979), and Shull and McKee (1979) have discussed the UV flux through the shock front. Shull and McKee's results for the equilibrium preionization are shown in Figure 3. Most radiative shock waves faster than perhaps 100

TABLE 2

FAMILY RELATIONSHIPS[a]

g_H	g_{He}	v_s (km s^{-1})	n_0 (cm^{-3})	B_0 (μG)
		$v_n = 200$ km s^{-1}		
1	1	200	5	0.05
0	0	186	5.8	0.058
		$v_n = 140$ km s^{-1}		
1	1	140	10	0.1
0.5	0.54	129.5	11.6	0.116
0	0	119	14.0	0.14
		$v_n = 100$ km s^{-1}		
1	1	100	19.6	0.2
0.5	0.7	85.6	26.5	0.27
		$v_n = 80$ km s^{-1}		
1	1	80	30.6	0.31
0.5	0.8	58.9	56.5	0.57

[a] $T_0 = 10^4$ K in all cases.

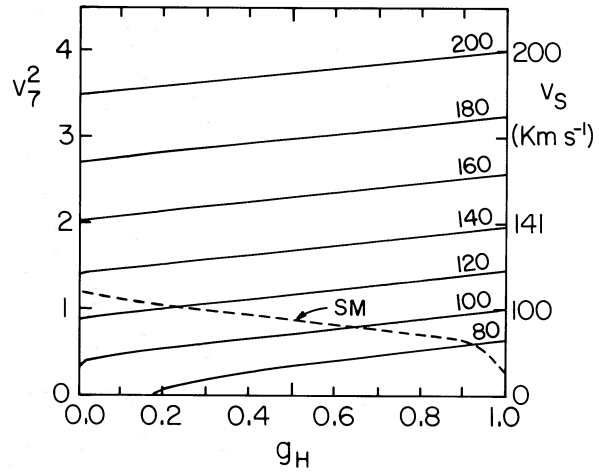

FIG. 3.—Equivalent shock families. Each curve represents one family of shock velocity vs. hydrogen neutral fraction. Corresponding helium neutral fraction follows from Fig. 2. Each curve is labeled with its value of v_n. Notice that vertical scale is quadratic in shock velocity. Left axis is labeled by $v_7^2 = (v_s/100 \text{ km s}^{-1})^2$. Dashed line labeled "SM" is Shull and McKee's (1979) equilibrium ionization concentration.

km s^{-1} have more ionizing photons emerging than ions being swept in. They should, in general, have a high degree of preionization. For supernova remnants, however, shock fronts faster than perhaps 170 km s^{-1} (depending very weakly on density) tend to be nonradiative—their deceleration time scales are shorter than their cooling time scales. Hence, a shock which decelerates rapidly from $v_0 > 200$ km s^{-1} will not have been producing significant UV for much of its previous history, and the preionization level can at first be much lower than an equilibrium calculation would suggest. This phenomenon must be responsible for the observed ionization zone radiation (S_1) in the otherwise nonradiative shocks discussed by Raymond *et al.* (1983).

Conversely, shocks which have slowed below 100 km s^{-1} tend to be encountering material which is, because of its long recombination time scale (10^5 yr/n), more preionized than in equilibrium. This recombination hysteresis implies that low-velocity shocks should rarely, if ever, be underionized.

There are also shock parameters existing in nature which are not represented on the diagrams. Since the region in which He^+ is excited and ionized cannot be separated from the S_2 "cooling" zone, we have assumed that helium is neutral or singly ionized in the preshock gas in all the models presented. At high shock velocities, this may be inappropriate. If a fraction $g_{He^{++}}$ of the preshock helium is fully ionized, a shock at velocity v_s should look *roughly* like an otherwise similar shock at v_s', with

$$v_s'^2 = v_s^2 + g_{He^{++}}(43 \text{ km s}^{-1})^2 .$$

(At high temperatures the singly ionized helium emission is $4A$ times that of hydrogen.)

The diagram further makes it clear that the family concept changes in character for initial conditions below the trajectory of the $v_n = 100$ km s^{-1} shock family. For $v_7^2 < 1 - 0.5(1 - g) = 0.5(1 + g)$, full ionization cannot be achieved by collisional processes. Furthermore, for situations close to this track, the S_2 spectrum may be very sensitive to the precise conditions. It can resemble any preionized shock slower than 70 km s^{-1}.

Figure 3 shows the equivalent shock velocity trajectory for $v_n = 80$ km s^{-1}. It never reaches $g_H = 0$. Nevertheless, along its trajectory it links initial conditions with at least roughly similar S_2 spectra. Looking at the diagram as showing loci of similar S_2 spectra, an immediate qualitative difference between preionized and non-preionized shocks is apparent. For $g(0) = 1$, all shocks faster than 100 km s^{-1} have corresponding family members with $g(0) = 0$. For $g(0) = 1$ and $v_0 \approx 100$ km s^{-1}, the corresponding $g(0) = 0$ member varies rapidly, suggesting a rapid change in the S_2 spectrum. Finally, for $g(0) = 1$ and $v_0 < 100$ km s^{-1}, the S_2 spectrum continues it evolution into a regime with no counterpart in preionized material.

V. FAMILY SPECTRA

The radiative shock wave code used to calculate the spectra of the family members of Table 2 is essentially that of Raymond (1979). It has been revised considerably, however, as described in Appendix C, and is ready for an updated exploration of parameter space.

The model results presented below, in addition to exploring the validity of family similarities, serve as a first overview of the new spectra. They all have essentially negligible magnetic field effects, and modest collisional de-excitation. (The pressures are roughly a factor of 4 higher than those commonly inferred for the Cygnus Loop.) The elemental abundances assumed are set A of Raymond (1979); the radiative transfer parameter R_{max} is 3 in every case.

One assumption built into the shock code (and therefore used in the simplified code described in Appendix A as well) may not be appropriate. We have taken the electron and ion temperatures to be always equal. Since nearly all of the kinetic energy of the preshock gas resides in the ions, the thermalization in the shock front gives nearly all the energy of the postshock gas initially to the ions. The electrons and ions will share the thermal energy by Coulomb collisions and perhaps much more rapidly by plasma turbulence (see McKee and Hollenbach 1980). We have assumed that T_e and T_i equilibrate rapidly compared with the hydrogen excitation and ionization time, through plasma processes in the shock.

As pointed out by Hamilton and Sarazin (1984) in the context of shocks in highly metal-enriched supernova ejecta, plasma turbulence is only effective in the very narrow shock front region, so electrons liberated later by ionization in the shocked gas probably reach equilibrium only on a Coulomb time scale. Itoh (1984) applies this idea to partially neutral preshock gas. Some observational evidence for electron-ion equilibration at the Coulomb rate is available from the study of a nonradiative shock in the Cygnus Loop (Raymond *et al.* 1983).

We will defer detailed investigation of Coulomb equilibration models to a future paper, but note that the Coulomb-dominated shocks would differ mostly in having values of R_H and R_{He} larger than in the instant equilibration models. The increase is modest at the upper end of the velocity range (cf. Raymond *et al.* 1983), but could be severe for the lowest velocities (Ohtani 1980).

Table 3 demonstrates that spectra of shocks *within* the four idealized families examined are extremely similar when line strengths are normalized to the recombination part of the Hβ emission. (No attempt has been made to fine tune the family membership using the full spectral code.) In the higher velocity families, relative line strengths typically differ by only 5%, with somewhat greater variation in the strengths of the highest temperature lines (easily improvable with fine tuning). The variation in relative line strengths is much larger in the low-velocity families because the separation between ionization and "cooling" regions is less clean. Nevertheless, the distinctions between families are far greater than those within them, even with no fine tuning. Our most significant conclusion is thus that the idealized families do provide a meaningful classification of spectra.

Judging from Table 3, one can unambiguously discriminate among families by taking the ratio of a high-temperature to a low-temperature line. The sensitivity of the line strengths is so great that modest abundance changes will have little effect. For the high velocity families: N V:C III] is appropriate, while for the low-velocity families [O III]:[O II] can be used. No single line ratio can be used over the whole velocity range because N V will be undetectable in slow shocks, while [O III]:[O II] saturates above 100 km s^{-1}.

It is also possible in principle to find the preshock neutral fraction quite easily from the [N II]:Hα ratio once the family has been determined. [To within the cross section uncertainties, $I(H\alpha) = 3I(H\beta)$.] There is, however, a serious ambiguity, in that a reduced N abundance may be difficult to tell from an increased preshock neutral fraction. In addition, the case A/case B differential introduces further uncertainty. These

TABLE 3

RUN PARAMETERS AND SPECTRA NORMALIZED TO RECOMBINATION PORTION OF Hβ = 100

A. RUN PARAMETERS

	RUN NUMBER								
FAMILY	1	2	3	4	5	6	7	8	9
v_n/v_i	200/186	200/186	140/119	140/119	140/119	100/–	100/–	80/–	80/–
v_s	200	186	140	130	119[a]	100	85.6	80	58.9
g_H	1	0	1	0.5	0	1	0.5	1	0.5

B. NORMALIZED LINE INTENSITIES

	RUN NUMBER								
SPECTRAL LINE	1	2	3	4	5	6	7	8	9
N v λ1240	354	315	5	5	8	...	...	...	...
O iv] λ1400	265	260	89	93	99	...	...	...	...
Si iv λ1400	35	33	150	146	121	5	15	...	...
N iv] λ1486	40	33	31	32	33	...	...	...	...
C iv λ1550	573	560	932	981	1040	1	1	...	...
He ii λ1640	28(100)	28(99)	22(97)	24(106)	27(113)	...	...	...	...
O iii] λ1666	152	144	158	160	155	3	5	...	...
N iii] λ1750	34	31	60	61	59	5	7	...	...
Si iii] λ1892	88	85	200	195	168	137	285	8	7
C iii] λ1909	171	169	577	582	533	125	204	31	4
C ii] λ2325	127	136	317	323	308	219	352	76	94
Mg ii λ2800	126	137	152	160	174	130	122	138	206
[O ii] λ3727	510	519	778	789	758	952	1230	368	381
[Ne iii] λ3969	36	36	56	57	56	9	4.9	...	...
[S ii] λ4070	29	30	37	38	38	21	25	8	16
[O iii] λ4363	23	22	26	27	26	1	1	...	...
He ii[b] λ4686	5(8)	5(8)	4(8)	5(9)	5(9)	...	...	...	...
Hβ[c] λ4861	129	102	157	130	103	286	204	277	178
[O iii] λλ5007, 4959	333	322	445	450	440	12	17	...	...
He i λ5876	6	5	8	8	7	3	3	1	1
[O i] λλ6300, 63	173	174	200	212	224	41	41	61	58
[N ii] λλ6548, 84	282	281	296	304	312	234	265	161	155
[S ii] λλ6717, 27	228	228	288	299	301	125	152	84	118
[O ii] λλ7320, 30	24	24	45	41	39	53	75	15	14
2γ continuum	2550	1800	3340	2600	1850	6750	4490	6510	3770

[a] Preshock density was 10 cm^{-3} rather than Table 2 value.
[b] Case A with case B in parentheses.
[c] Case B: $I(H\alpha) = 3I(H\beta)$.

are potentially serious problems for attempts to derive abundances from optical spectra of supernova remants (e.g., Binette *et al.* 1982; Dennefeld and Kunth 1981; Blair *et al.* 1985). In the ultraviolet, the ratio of a line such as O III] to the hydrogen two-photon continuum is less sensitive to abundance uncertainties. (The fact that hydrogen is not a significant coolant in the ultraviolet line-emitting region makes the energy radiated in lines like O III] almost abundance independent for constant relative abundances of important coolant elements. Helium, however, is an important confounder.)

This method seems to work for data of existing quality. Ultraviolet spectra of Miller's (1974) position 1 in the Cygnus Loop are given by Benvenuti, Dopita, and D'Odorico (1980). The line to two-photon continuum ratio in this complex region suggests a preshock neutral fraction near 0.5, in agreement with the model for position 1 given by Binette *et al.* (1982). The morphology of this position is extremely complicated, and a mixture of shock velocities may well be present, but the inference of significant preshock neutral fraction depends only on the need for collisional excitation to explain the high two-photon to Hβ ratio. The *IUE* spectra for Miller's position 3 and Fesen, Blair, and Kirshner's (1982) position Y in the Cygnus Loop, and a filament in the Vela supernova remnant (Raymond *et al.* 1980, 1981), on the other hand, indicate very low preshock neutral fractions with otherwise comparable UV spectra. Ultraviolet spectra of Herbig-Haro objects indicate a substantial component of collisionally excited two-photon emission (Dopita, Binette, and Schwartz 1982; Brugel, Shull, and Seab 1982), although detailed interpretation is complicated by the range of shock velocities present in the bow shock (Hartmann and Raymond 1984).

Another diagnostic for preshock neutral fraction would be a ratio of He I singlet to triplet lines, since the singlets are strong in collisionally excited gas, while the triplets are strong in recombining gas. Such an enhancement has been detected in the spectrum of a nonradiative shock in the Cygnus Loop (Raymond *et al.* 1983), but has not been reported in spectra of radiative shocks. The disadvantage of such a line ratio is the need for accurate measurement of weak lines.

The optical spectra of runs 1–5, representing the two families $v_n = 200$ and 140 km s^{-1}, are extremely similar. The calculation at constant photoionization zone density has clarified the asymptotic character of the S_3 spectrum at high shock velocities. The differences between the two families in the UV is

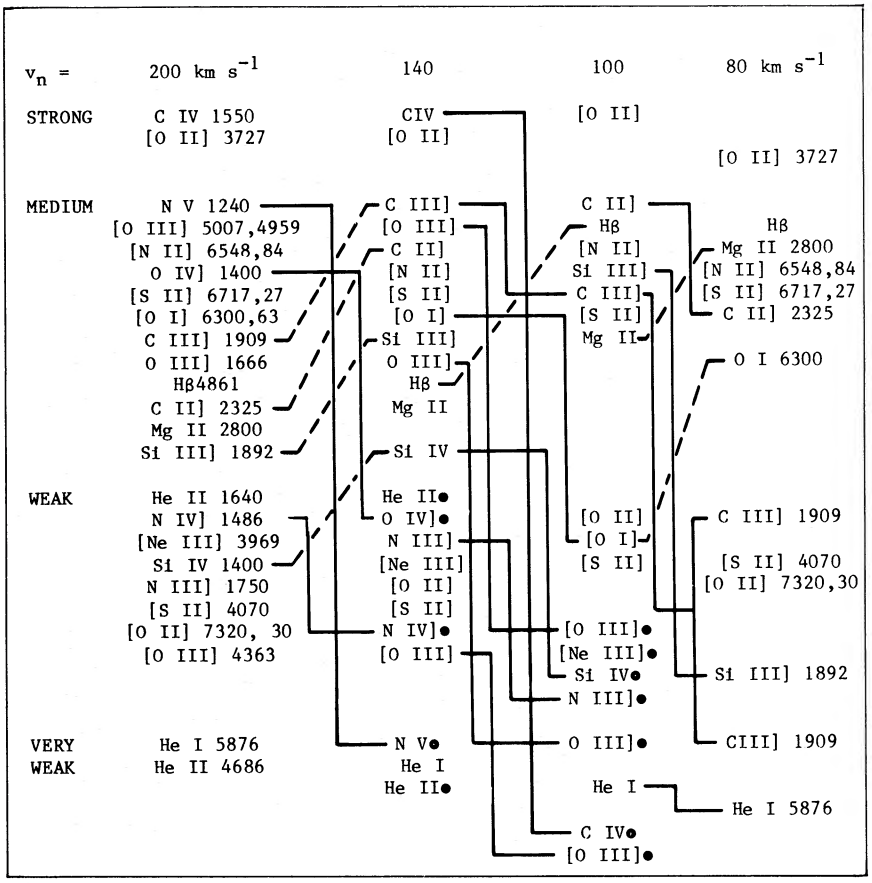

FIG. 4.—The family spectra ordered by line strength. Connections and large dots show lines whose comparative strength changes appreciably between families, dashed lines for increases, solid for decreases, and large dots if the line is not found in the next lower v_n family. Note that He II λ1640 is shown for the average of cases A and B.

quite apparent, however. Future efforts concentrating on the pressure and abundance dependencies of the optical spectrum should clarify the information content of S_3.

Although single line ratios can be used as described above to identify family membership, one should not lose sight of the fact that from family to family the variation is one of richness of the spectrum, gaining lines of progressively higher excitation in moving from lower to higher v_n cases. This richness variation is stressed in Figure 4, which shows the different family spectra in classes of decreasing line strength. The connections and large dots indicate those lines which change intensity significantly between families, and are therefore most useful in precise family determination. But the other lines are equally important in confirming the overall propriety of the model. In fact, a table such as this, with more finely spaced entries, should provide a family identification method which would utilize all available information qualitatively while remaining indifferent to moderate abundance variations. Methods of nonparametric comparison could thus be very useful tools. Between v_n = 200 and 140 km s^{-1}, N V, O IV], and N IV] lines all drop precipitously, while C III], C II], and Si IV all rise in significance. Similarly, between 140 and 100 km s^{-1}, C IV, C III], [O III], [O I], O III], Si IV, N III], O IV], N IV], He II 1640, N V, and He II 4686 lines all drop, while only Hβ increases. Finally, between 100 and 80 km s^{-1}, C II], Si III], C III], [O III], [Ne III], Si IV, N III], O III], He I, and C IV lines drop, while Mg II and [O I] increase.

Considerable further work is required in developing the usefulness of the family concept, shown herein to merit the attention. This includes running a more closely spaced model grid, sets with different recombination zone densities and different abundances, and investigating the delay of electron temperature equilibration for cases with appreciable neutral content. In addition, we plan to examine the S_3 spectra as functions of the completeness of the photoionization zone to establish quantitative criteria for that completeness.

This material is based upon work supported by the National Science Foundation under grant AST 84-15142.

D. P. C. would like to acknowledge useful conversations with Jeff Hester, and is grateful for support from the Smithsonian Institution at CfA during 1983 May when the family concept was invented. He was also supported in part by the Space Physics and Astronomy Department at Rice University, and by NASA grant NGL 50-002-044 to the University of Wisconsin. He is further grateful for the patience of his wife during periods without support.

J. C. R. acknowledges useful conversations with Bill Blair. His efforts were supported in part by NASA grant NAG 5-87.

APPENDIX A

EVOLUTION OF THE IONIZATION ZONE

The detail of the collisional ionization zone is straightforward, particularly when the hydrogen neutral fraction is used as the independent variable. Starting with the basic relationships:

$$h = \frac{1}{2} m_{\rm H} \frac{(1+4A)}{1+A} v^2 + \frac{B^2}{4\pi n} + \frac{5}{2}\left(1 + \frac{n_e}{n}\right)kT + \frac{(1-g_{\rm H})I_{\rm H} + A(1-g_{\rm He})I_{\rm He}}{1+A}$$

for the enthalpy per particle,

$$p_s = \frac{B_0^2}{8\pi} + \frac{2 - g_{\rm H}(0) + A[2 - g_{\rm He}(0)]}{1+A} n_0 kT_0 + m_{\rm H} \frac{(1+4A)}{1+A} n_0 v_0^2$$

for the stagnation pressure,

$$n = xn_0\,, \qquad v = \frac{v_0}{x}\,, \qquad p_T \equiv (n + n_e)kT = p_s - \frac{B^2}{8\pi} - \rho v^2\,, \qquad B = xB_0$$

from mass, momentum, and magnetic flux conservation, introducing the three rate equations,

$$\frac{dg_{\rm H}}{dt} = -n_e g_{\rm H} C_{\rm H}(T)\,, \qquad \frac{dg_{\rm He}}{dt} = -n_e g_{\rm He} C_{\rm He}(T)\,, \qquad \frac{dh}{dt} = -n_e\left(\frac{r_{\rm H} g_{\rm H} + A r_{\rm He} g_{\rm He}}{1+A}\right),$$

and defining the auxiliary parameters,

$$R = \frac{g_{\rm He}}{g}\,, \qquad Q_1 = \frac{5}{2}\frac{p_s}{n_0 x^2} + \frac{B_0^2}{16\pi n_0} - \frac{4(1+4A)m_{\rm H} v_0^2}{(1+A)x^3}\,, \qquad Q_2 = \frac{r_{\rm H} + C_{\rm H} I_{\rm H}}{(1+A)C_{\rm H}} + RA\frac{r_{\rm He} + C_{\rm He} I_{\rm He}}{(1+A)C_{\rm H}}\,,$$

the evolution equations are simply

$$\frac{d\ln x}{d\ln g_{\rm H}} = -\frac{g_{\rm H}}{x}\frac{Q_2}{Q_1}\,, \qquad \frac{d\ln R}{d\ln g_{\rm H}} = \frac{C_{\rm He}}{C_{\rm H}} - 1\,.$$

Only these two equations need be integrated, providing x and R. The remaining parameters follow algebraically:

$$g_{\rm He} = Rg_{\rm H}\,, \qquad h = \frac{(1-g_{\rm H})I_{\rm H} + A(1-g_{\rm He})I_{\rm He}}{1+A} + \frac{5}{2}\frac{p_s}{xn_0} - \frac{B_0^2 x}{16\pi n_0} - 2m_{\rm H}\left(\frac{1+4A}{1+A}\right)\frac{v_0^2}{x^2}\,,$$

$$p_T = p_s - \frac{B_0^2 x^2}{8\pi} - \frac{\rho_0 v_0^2}{x}\,, \qquad \chi \equiv \frac{n+n_e}{n} = 2 - \frac{g_{\rm H} + Ag_{\rm He}}{1+A}\,, \qquad T = \frac{p_T}{\chi nk} = \left[\frac{p_s}{xn_0} - \frac{B_0^2 x}{8\pi n_0} - m_{\rm H}\left(\frac{1+4A}{1+A}\right)\frac{v_0^2}{x^2}\right]\Big/(\chi k)\,.$$

After each integration step, the revised value of T is used to update the rate coefficients: $C_{\rm H}$ and $C_{\rm He}$ for ionization, $r_{\rm H}$ and $r_{\rm He}$ for cooling. The energy output in the various modes is found by taking fractions of the total loss $-\Delta h$ in the step

$$\Delta E_{\rm Hi} = \frac{r_{\rm Hi} g_{\rm H}}{r_{\rm H} g_{\rm H} + A r_{\rm He} g_{\rm He}}(-\Delta h)\,, \qquad \Delta E_{\rm Hei} = \frac{A r_{\rm Hei} g_{\rm He}}{r_{\rm H} g_{\rm H} + A r_{\rm He} g_{\rm He}}(-\Delta h)\,.$$

Running sums of these outputs thus provide the mode energy output per average ion.

APPENDIX B

INVERSION TO EQUIVALENT SHOCK PARAMETERS

Since each point along the evolutionary track in the ionization zone consists of yet another member of the same family, it is useful to perform a running inversion to obtain the shock parameters leading to the intermediate states. The initial conditions of the first member of the family are n_0, $g_{\rm H}(0)$, $g_{\rm He}(0)$, T_0, v_0, B_0. Also useful is $\chi_0 = \{2 - g_{\rm H}(0) + A[2 - g_{\rm He}(0)]\}/(1+A)$. The post shock evolution takes us to a state with $n = xn_0$, $B = xB_0$, $v = v_0/x$, T, g, $g_{\rm He}$, and χ, and we are interested in inverting to a mock preshock condition with the same h, g, $g_{\rm He}$, T_0, stagnation pressure, and B/n. Defining the mock initial density to be $n_i = yn_0$, then $B_i = yB_0$. Enthalpy conservation implies

$$\frac{mv_0^2}{2x^2} + x\frac{B_0^2}{4\pi n_0} + \frac{5}{2}\chi kT = \frac{mv_i^2}{2} + y\frac{B_0^2}{4\pi n_0} + \frac{5}{2}\chi kT_0\,,$$

where the ionization energy is the same on both sides and was omitted. Stagnation pressure equivalence requires

$$mn_0 v_0^2 + \chi_0 n_0 kT_0 + \frac{B_0^2}{8\pi} = ymn_0 v_i^2 + yn_0 \chi kT_0 + y^2\frac{B_0^2}{8\pi}\,.$$

These coupled equations can be solved for both v_i and y. Defining

$$b = \frac{mv_0^2}{x^2} + x\frac{B_0^2}{2\pi n_0} + 5\chi k(T - T_0) + \chi kT_0 , \qquad c = \left(mv_0^2 + \chi kT_0 + \frac{B_0^2}{8\pi n_0}\right)\frac{B_0^2}{8\pi n_0} , \qquad f = mv_i^2 + \chi kT_0 , \qquad g = y\left(\frac{B_0^2}{8\pi n_0}\right) ,$$

the equations reduce to $b = f + 4y$, $c = g(f + g)$, making

$$g = \frac{b - (b^2 - 12c)^{1/2}}{6} , \qquad y = \frac{g}{[(B_0^2)/(8\pi n_0)]} , \qquad f = b - 4g ,$$

$$v_i = \left[\frac{1}{m}(f - \chi kT_0)\right]^{1/2} , \qquad n_i = yn_0 , \qquad B_i = yB_0 .$$

In the limit of negligible preshock temperature and magnetic field,

$$mv_i^2 \approx 5\chi kT + \frac{mv_0^2}{x^2} , \qquad y \approx \frac{v_0^2}{v_i^2} .$$

APPENDIX C

MODIFICATIONS TO THE RADIATIVE SHOCK CODE

The treatment of hydrodynamics and radiative transfer is unchanged since the description in Raymond (1979). Major changes have been made to many of the atomic rates:

Charge transfer: as described in Butler and Raymond (1980).

Photoionization cross sections: those considered uncertain (mostly high Z or highly ionized species) have been replaced by Reilman and Manson (1979) cross sections. A four-term polynomial fit is used.

Collisional ionization: the distorted wave calculations of Younger (1981) are used instead of the Summers (1974) rates used previously. The new rates are generally intermediate between the Summers rates and the Lotz (1967) rates. Ionization from metastable levels is explicitly calculated though the effects are negligible at interstellar densities.

Dielectronic recombination: low-temperature dielectronic recombination rates from Nussbaumer and Storey (1984) are used when available. The effects of autoionization to excited levels are estimated from the results of Smith *et al.* (1984). Density sensitivity is included through fits to the tables of Summers (1974), but this effect is negligible at interstellar densities.

Collisional excitation: many collision strengths are taken from the compilation of Merts *et al.* (1980), their inclusion of the distorted wave calculations of Mann and Bhatia being especially useful. When available, close coupling calculations including resonances are used. Sources include Aggarwal (1983; H^0), Fon, Berrington, and Burke (1981; He^0), Dufton *et al.* (1978; C III, O V), Baluja *et al.* (1980, 1981; O III, Si III), Pradhan, Norcross, and Hummer (1981; He sequence), Pradhan (1976; S II), Van Wyngaarden and Henry (1981; S V), Bhadra and Henry (1980; S IV), Bhatia, Doschek, and Feldman (1980; S IV), Nussbaumer and Storey (1980; Fe II), and Garstang, Robb, and Rountree (1978; Fe III). Note that more reliable excitation rates are available for the $n = 3$ level of hydrogen than for $n = 4$, so we have used the $n = 3$ rates to compute Hα excitation and *assumed* $I(\mathrm{H}\alpha)/I(\mathrm{H}\beta) = 3$ for collisional excitation. (The decrement would be steeper for situations intermediate between cases A and B.) For two-photon emission we use the calculations of Benvenuti, Dopita, and D'Odorico (1980).

The He II emission lines were computed for both cases A and B. The excitation rates for λ4686 are more uncertain than those for λ1640, and the assumption of case B may significantly overestimate these line fluxes, since some of the He II Lyman line photons will escape or ionize H^0 or He^0.

REFERENCES

Aggarwal, K. M. 1983, *M.N.R.A.S.*, **202**, 15.
Baluja, K. L., Burke, P. G., and Kingston, A. E. 1980, *J. Phys. B*, **13**, 829.
———. 1981, *J. Phys. B*, **14**, 119.
Benvenuti, P., Dopita, M., and D'Odorico, S. 1980, *Ap. J.*, **238**, 601.
Bhadra, K., and Henry, R. J. W. 1980, *Ap. J.*, **240**, 368.
Bhatia, A. K., Doschek, G. A., and Feldman, U. 1980, *Astr. Ap.*, **86**, 32.
Binette, L., Dopita, M. A., D'Odorico, S., and Benvenuti, P. 1982, *Astr. Ap.*, **115**, 315.
Blair, W. P., Kirshner, R. P., and Chevalier, R. A. 1985, *Ap. J.*, submitted.
Blair, W. P., and Raymond, J. C. 1984, *Bull. AAS*, **15**, 930.
Brugel, E. W., Shull, J. M., and Seab, C. G. 1982, *Ap. J. (Letters)*, **262**, L35.
Butler, S. E., and Raymond, J. C. 1980, *Ap. J.*, **240**, 680.
Chevalier, R. A., Kirshner, R. P., and Raymond, J. R. 1980, *Ap. J.*, **235**, 186.
Cox, D. P. 1972, *Ap. J.*, **178**, 143.
Dennefeld, M., and Kunth, D. 1981, *Astr. Ap.*, **86**, 989.
Dopita, M. A., Binette, L., and Schwartz, R. D. 1982, *Ap. J.*, **161**, 183.
Dufton, P. L., Berrington, K. A., Burke, P. G., and Kingston, A. E. 1978, *Astr. Ap.*, **62**, 111.
Fesen, R. A., Blair, W. P., and Kirshner, R. P. 1982, *Ap. J.*, **262**, 171.
Fon, W. C., Berrington, K. A., and Burke, P. G. 1981, *J. Phys. B*, **14**, 2921.
Garstang, R. W., Robb, W. D., and Rountree, S. P. 1978, *Ap. J.*, **222**, 384.
Hamilton, A. J. S., and Sarazin, C. L. 1984, *Ap. J.*, **287**, 282.
Hartmann, L., and Raymond, J. C. 1984, *Ap. J.*, **276**, 560.
Itoh, H. 1984, *Ap. J.*, **285**, 601.
Lotz, W. 1967, *Ap. J. Suppl.*, **14**, 207.
McKee, C. F., and Hollenbach, D. J. 1980, *Ann. Rev. Astr. Ap.*, **18**, 219.
Merts, A. L., Mann, J. B., Robb, W. D., and Magee, N. W., Jr. 1980, Los Alamos Informal Rept. No. LA-8267-MS.
Miller, J. S. 1974, *Ap. J.*, **189**, 239.
Nussbaumer, H., and Storey, P. J. 1980, *Astr. Ap.*, **89**, 308.
———. 1984, *Astr. Ap. Suppl.*, **56**, 293.
Ohtani, W. 1980, *Pub. Astr. Soc. Japan*, **32**, 11.
Pradhan, A. K. 1976, *M.N.R.A.S.*, **177**, 31.
Pradhan, A. K., Norcross, D. W., and Hummer, D. G. 1981, *Ap. J.*, **246**, 1031.
Raymond, J. C. 1979, *Ap. J. Suppl.*, **39**, 1.
Raymond, J. C., Black, J. H., Dupree, A. K., Hartmann, L., and Wolff, R. S. 1980, *Ap. J.*, **238**, 881.
———. 1981, *Ap. J.*, **246**, 100.
Raymond, J. C., Blair, W. P., Fesen, R. A., and Gull, T. R. 1983, *Ap. J.*, **275**, 636.
Reilman, R. F., and Manson, S. T. 1979, *Ap. J. Suppl.*, **40**, 815.
Shull, J. M., and McKee, C. F. 1979, *Ap. J.*, **227**, 131.
Smith, B. W., Raymond, J. C., Mann, J. B., and Cowan, R. D. 1985, *Ap. J.*, in press.
Summers, H. P. 1974, Appleton Lab. Internal Memo 367.
Van Wyngaarden, W. L., and Henry, R. J. W. 1981, *Ap. J.*, **246**, 1040.
Younger, S. M. 1981, *J. Quant. Spectrosc. Rad. Transf.*, **26**, 329.

DONALD P. COX: Department of Physics, University of Wisconsin, 1150 University Avenue, Madison WI 53706

JOHN C. RAYMOND: Center for Astrophysics, 60 Garden Street, Cambridge, MA 02138